Effect of Shear on the Face-Centered Cubic Phase in a Diblock Copolymer Gel

Christophe Daniel and Ian W. Hamley*

School of Chemistry, University of Leeds, Leeds LS2 9JT, U.K.

Withawat Mingvanish and Colin Booth

Department of Chemistry, University of Manchester, Manchester M13 9PL, U.K.

Received August 24, 1999; Revised Manuscript Received January 21, 2000

ABSTRACT: The effect of steady or oscillatory shear on the orientation of a face-centered cubic micellar phase formed by a poly(oxyethylene)−poly(oxybutylene) diblock copolymer in an aqueous salt solution has been investigated using small-angle X-ray scattering (SAXS). Steady shear was found to orient the mesophase into a polydomain structure with the hexagonal close-packed (hcp) planes both parallel and perpendicular to the shear plane. The hcp layers were found to be randomly stacked along the shear gradient direction. Different flow mechanisms were also observed as the shear rate was increased. At $\dot{\gamma} = 5\ s^{-1}$ a sliding mechanism of the 2D hcp layers stacked perpendicular to the shear gradient direction was identified. This produced an increase in domain spacing compared to that for an unoriented gel that is consistent with a transition from an fcc powder to sliding hcp layers. At $\dot{\gamma} = 50\ s^{-1}$ a partial reorientation of the {111} planes oriented perpendicular to the shear plane was observed. Upon cessation of shear, melted grains recrystallized in a distinct orientation of an fcc crystal with a [110] direction parallel to the shear. Partial melting of grains with {111} planes oriented parallel to the shear plane only occurred at $\dot{\gamma} = 250\ s^{-1}$. The effect of strain amplitude of oscillatory shear was investigated at constant shear rate on samples preoriented by steady shear. The behavior noted for steady shear, specifically, partial reorientation of {111} planes was only observed in the limit of very large strain amplitudes.

1. Introduction

Block copolymers dissolved in a selective solvent can form micelles above a critical micelle concentration[1] (cmc), and solutions display viscoelastic fluid properties due to a liquidlike organization of the micelles. When the copolymer concentration is increased above a critical gelation concentration (cgc), the micelles can self-assemble into ordered structures leading to the formation of a liquid crystalline phase such as a cubic phase of spherical micelles, a hexagonal phase of rodlike micelles, or a lamellar phase. In contrast to micellar solutions, these structures display a finite yield stress. The nature of the ordered structure formed depends on the copolymer structure, its concentration, and the temperature. Solutions of block copolymers can display a very rich phase behavior and this topic has been widely studied.[1−5] Of particular interest is the formation of cubic micellar phases above the cgc. It has been observed that the development of a cubic phase may lead to the formation of a hard gel with a high dynamic shear modulus, e.g., $G' \sim 10^4$ Pa.[6] The presence of a cubic phase is characterized by one of two arrangements of micelles, either face-centered cubic (fcc) or body-centered cubic (bcc). The formation of a fcc phase or a bcc phase depends on the relative length of blocks forming the corona and the core of the spherical micelles. For short corona blocks, the formation of the fcc structure is favored whereas for long corona blocks the bcc structure is favored.[7−9]

Recently, the orientation and the structure of cubic-packed micellar copolymer gels under flow have created a great deal of interest and numerous reports have been published on this subject. The first studies showing the orientation of block copolymer micellar solution under steady shear were performed with poly(oxyethylene)−poly(oxypropylene)−poly(oxyethylene) (EPE) gels characterized by a bcc structure. Simultaneous shear and SANS measurements showed that steady shear flow can lead to highly oriented structures with the shear gradient along a [111] direction and shear flow parallel to a [112] direction.[10,11]

The analogy between sheared copolymer micellar solutions with a cubic structure and sheared crystals of colloidal sols has also been mapped out.[12] Solutions of poly(styrene)−poly(isoprene) diblocks in decane with either a bcc structure or a fcc structure were submitted to different steady shear rates while SANS measurements were performed in situ.[10,11] Results showed that under shear a bcc micellar solution developed a twinned structure with the {110} layers normal to the shear gradient as in colloidal bcc crystals[13] and for both systems flow occurred along the twinning planes. For the fcc-packed micellar structure a transition from polycrystallinity to {111} sliding layers was observed when increasing the shear rate.[12] This behavior is similar to colloidal fcc crystals subjected to shear for which layers of hexagonal (hcp) are stacked perpendicular to the shear gradient and a close packed direction is parallel to the flow direction.[14−17] Furthermore, excellent agreement was observed between experimental diffraction patterns and calculated diffraction patterns obtained[12] using the model developed by Loose and Ackerson[18] for sliding hcp layers in colloidal crystals. Since then, the so-called layer-sliding regime has also been observed in other micellar crystals with a cubic structure.[19,20] Beside the layer sliding mechanism, other flow behaviors have also been reported in micellar cubic crystals, and the transitions between shearing flows

* Author for correspondence.

10.1021/ma991444m CCC: $19.00
Published on Web 03/03/2000

were investigated. For a solution of an EPE triblock forming a fcc phase, different flow mechanisms were observed as the shear rate was increased.[21,22] It was found that, at low shear rate, the EPE gel flowed as a polycrystal phase of oriented microdomains and the shear gradient was localized at the interfaces between the microdomains and between defects. When the shear rate was increased, the layer sliding mechanism was observed, and at higher shear rate, melting of the structure occurred.

In this paper, we report on the effect of shear on the orientation of a fcc phase formed in a gel of a poly(oxyethylene)−poly(oxybutylene) (EB) diblock, $E_{55}B_8$ in 0.2 M K_2SO_4 solution. Here and elsewhere the subscripts for a diblock E_mB_n denote the number of repeat units. The sample of $E_{55}B_8$ was subjected to steady shear and oscillatory shear in a Couette cell while small-angle X-ray scattering (SAXS) patterns were recorded simultaneously. Though the effect of shearing on the orientation of the bcc phase formed in EB diblock gels has been investigated in detail,[20,23−27] the effect of shear on the fcc phase of EB diblock copolymer gel has been less well studied. In particular, a detailed comparison of the effect of steady shear vs oscillatory shear has yet to be made.

For a bcc phase formed in a solution of $E_{90}B_{10}$ subjected to large amplitude oscillatory shear, it was shown that low-frequency shear leads to a polydomain structure with grains containing {110} planes parallel to the shear plane and grains with {200} planes oriented perpendicular to the flow direction.[23] At higher frequency ($\omega = 100$ rad s^{-1}) a transition in orientation occurred and a [111] direction was found to be parallel to the shear direction with flow in {110} and {211} planes.[23] For steady shear flows, the same orientation was obtained for a shear rate above a critical shear rate $\dot{\gamma} = 50\ s^{-1}$, [24,25] and twinning of the crystal along the [111] direction was observed.[25] The study of the macroscopic orientation of the bcc phase showed that the alignment occurs through a slip-stick flow mechanism in the {110} planes in the [111] direction.[25]

The effect of shear was also investigated to a lesser extent for the fcc phase formed in EB copolymer gels.[20,26,27] Results for solutions of $E_{40}B_{10}$ subjected to steady shear showed that under shear the fcc structure forms a highly twinned structure with a random stacking of the hcp planes along the shear gradient.[26,27] It was found that an appreciable proportion of hcp planes are oriented perpendicular to the shear plane. Oscillatory shear led to an oriented fcc gel of $E_{40}B_{10}$,[20] although in that study, using a planar shear sandwich geometry, only low shear rates could be accessed.

To gain a better knowledge of the shear effect on the fcc phase formed in EB micellar solutions, a $E_{55}B_8$ gel was subjected to steady shear and oscillatory shear in a Couette cell, which permits access to a wide range of shear rates (and amplitudes for oscillatory shear).[28] Structural changes were recorded in situ using small-angle X-ray scattering.

2. Experimental Section

2.1. Materials. Copolymer $E_{55}B_8$ was synthesized by sequential anionic polymerization of ethylene oxide followed by 1,2-butylene oxide. A full description of the vacuum line and ampule methods employed can be found elsewhere[29,30] The monofunctional initiator was 2(2-methoxyethoxy)ethanol activated by reaction with potassium metal (mole ratio OH/K ≈ 10). Characterization of the copolymers was by gel permeation chromatography calibrated with poly(oxyethylene) standards which gave a reliable value of the ratio of mass-average to number-average molar mass, $\bar{M}_w/\bar{M}_n = 1.03$ without correction for instrumental effect, indicative of a narrow chain length distribution. ^{13}C NMR together with the assignments of Heatley et al.[31] was used to obtain absolute values of chain length (hence the number-average molar mass) and the composition. This involved comparison of the intensities of resonance from the carbons of end and backbone groups for the poly(oxyethylene) precursor from stage one of the polymerization and for the final copolymer, and of the CH_2 and CH carbons of the copolymer (for composition). Further comparison with the intensities of resonance of the carbons of the EB junctions confirmed the diblock structure and the purity of the product. The formula obtained was $E_{55}B_8$, for which we estimate an uncertainty in block length of ±2%.

The diblock copolymer gel described in this report was a 20 wt % gel in 0.2 mol dm^{-3} K_2SO_4 aqueous solution, which was prepared by mixing at 60−70 °C until complete dissolution of the copolymer gave a clear and homogeneous solution. Preparation was followed by several days storage in a refrigerator. The reason for preparing the gel with salt solution rather than pure water was to use the poorer solvent to compress the poly(oxyethylene) blocks of the micelle corona and in this way to favor formation of the fcc phase.[9,32,33]

2.2. Techniques. Small-angle X-ray scattering experiments were performed at the Synchrotron Radiation Source, Daresbury Laboratory, Daresbury, U.K. Beam-line 2.1 was used with an X-ray wavelength $\lambda = 1.5$ Å. The SAXS patterns were recorded on a multiwire gas-filled area detector located 3 m from the samples. A scattering pattern from an oriented specimen of wet collagen (rat tail tendon) was used for the calibration of the q scale range, ($q = 4\pi(\sin\theta)/\lambda$, where the scattering angle is defined as 2θ).

Samples were sheared in a homemade Couette cell, made of polycarbonate, that is described in detail elsewhere.[28] The couette cell consists of an outer cylindrical rotor and a central stator. The diameter of the stator is 50 mm and the size of the annular gap between both cylinders of the cell is 0.5 mm. The accessible shear rate range is $0.025 < \dot{\gamma}/s^{-1} < 525$ for continuous shear and $0.025 < \dot{\gamma}/s^{-1} < 525$ for the oscillatory shear mode within a shear amplitude range of $2 < \alpha/° < 3600$. As the Couette cell gap is much less than the radius of the stator, we can neglect the curvature of the cylinders, and the shear strain is given by $A = (2\pi\alpha/360)[(R_{stator} + R_{rotor})/(2(R_{rotor} - R_{stator})]$. All experiments were carried out in the so-called radial configuration for which the X-ray beam was incident along the shear gradient direction $\nabla\mathbf{v}$. This configuration provides SAXS patterns in the reciprocal space plane (q_v,q_e) where $\mathbf{v}$ indicates the shear velocity direction and $\mathbf{e} = \nabla\mathbf{v} \times \mathbf{v}$ the neutral (vorticity) direction.

Measurements were carried out at $T = 20$ °C with the temperature of the circulating fluid held constant by a Lauda CP-6 refrigerated heater/cooler bath.

3. Results and Discussion

3.1. Layer Structure Scattering Theory. As most of our results will be discussed in terms of 2D hcp layer stacking and layer sliding, it is useful to review briefly the model developed by Loose and Ackerson[18] (LA model) for the analysis of scattering data from such layered structures.

For a stacking of 2D hcp layers the scattering intensity is given by

$$S(\mathbf{q}) = \frac{1}{M}L(\mathbf{q})\left\langle\sum_{n=1}^{M}\sum_{m=1}^{M}\exp(i\mathbf{q}\cdot(\mathbf{R}_m - \mathbf{R}_n))\right\rangle \qquad (1)$$

where M specifies the number of layers in the crystal, $L(\mathbf{q})$ is the layer form factor and $\mathbf{R}_i$ represents the position of the origin of the ith layer.

Starting from 2D hcp stacking, different 3D hcp structures can be obtained according to the correlation between layers. Two possibilities exist for stacking the

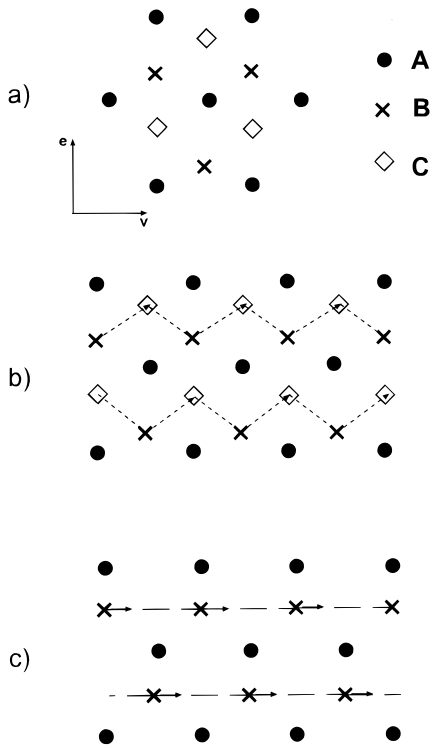

Figure 1. (a) An ABCABC... stacking sequence of hcp planes along the shear gradient direction. (b) Zigzag motion of a 2D hcp layers (×) with respect to a reference layer (●).[18] (c) Sliding mechanism of two neighboring layers.[18]

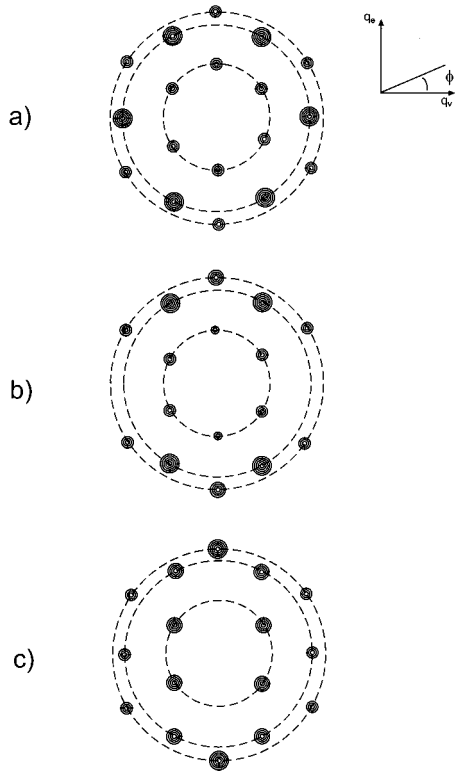

Figure 2. Schematic diffraction patterns according to Loose and Ackerson[18] for (a) highly twinned fcc crystal or random stacking, (b) the structure in zigzag motion at small shear rate, and (c) the structure under layer sliding mechanism. The size of the symbol schematically indicates the relative intensity of the reflections.

second 2D hcp layer such that it lies in hollow sites of the first one. These two layer stacking possibilities are referred as B and C. A perfect fcc structure can be characterized by a sequence ABCABC..., whereas sequences ABAB... and ACAC... represent a perfect 3D hcp structure (Figure 1a).

For a crystal composed of 2D hcp layers and containing stacking faults, the scattered intensity is given by[18]

$$S(\mathbf{q}) = L(\mathbf{q}_{\|})a(1-a)\left[1-\cos\left(2\pi\frac{2k-h}{3}\right)\right]\Big/ \left[2(1-2a)(1-\cos^2 q_{\perp} d\sqrt{2/3}) + 3a^2 - 4a^2(-1)^h \times \cos\left(2\pi\frac{2k-h}{6}\right)\cos q_{\perp} d\sqrt{2/3} + a^2\cos\left(2\pi\frac{2k-h}{3}\right)\right] \quad (2)$$

where a is the fraction of stacking faults, d is the nearest neighbor distance, $\mathbf{q}_{\|}$ is the component of $\mathbf{q}$ in the 2D hcp reciprocal plane, $q_{\perp}$ is the coordinate of $\mathbf{q}$ perpendicular to the 2D hcp reciprocal plane, and h, k are the Miller indices of the diffraction peaks of the 2D hcp lattice.

The case $a = 1$ corresponds to a perfect fcc crystal and $a = 0$ to a perfect 3D hcp structure whereas $a = 0.5$ corresponds to a random stacking of the layers. For values of h, k with $h - k = 3n$ (where n is an integer) the scattering intensities are independent of the number of stacking faults whereas for $h - k = 3n \pm 1$ stacking has a strong effect on the scattering intensities. In particular, eq 2 shows that the first-order reflections (h, k = 1, 0) are suppressed for a perfect fcc crystal. On the basis of eq 2, it is possible to anticipate the scattering patterns for oriented fcc crystals with different stacking sequences. The scattering pattern obtained with $q_{\perp} = 0$, i.e., when the incident beam is normal to the hcp layers, for the case of a random stacking or a highly twinned fcc crystal is schematically illustrated in Figure 2a.

When the close packed crystal is subjected to shear, with the shear gradient normal to the 2D hcp layers, different behaviors can be observed according to the shear rate. At small shear rates the motion of a layer with respect to a reference layer is a zigzag path between the two possible fcc configurations (Figure 1b).[18] When the shear rate is increased, the path becomes linear (Figure 1c) in the so-called layer sliding regime.[18] The scattering patterns calculated for random stacking or highly twinned fcc crystals for the two shear rate regimes are shown respectively in parts a and b of Figure 2. The main features that result from shearing are the decrease and eventual extinction of the meridional reflections of the inner ring whereas the meridional reflections of the third-order ring are enhanced. We also note the diffraction pattern is arranged in so-called "layer lines".

3.2. Steady Shear Orientation. SAXS patterns were obtained both for the gel under shear at different rates, and at rest following each period of shearing. The shear was increased incrementally from $\dot{\gamma} = 5\ s^{-1}$ to $\dot{\gamma} = 500\ s^{-1}$. Figures 3−5 show, respectively, the two-dimensional SAXS patterns obtained in the (q_v, q_e) plane, the reduction of the 2D data to a plot of intensity vs q, and the azimuthal intensity profiles of the first-order peak. The reduction of the 2D data was obtained by radial integration of the two-dimensional pattern with $q_e \geq 0$. Only half of each pattern was used, since the lower portion was partly obscured in some cases due

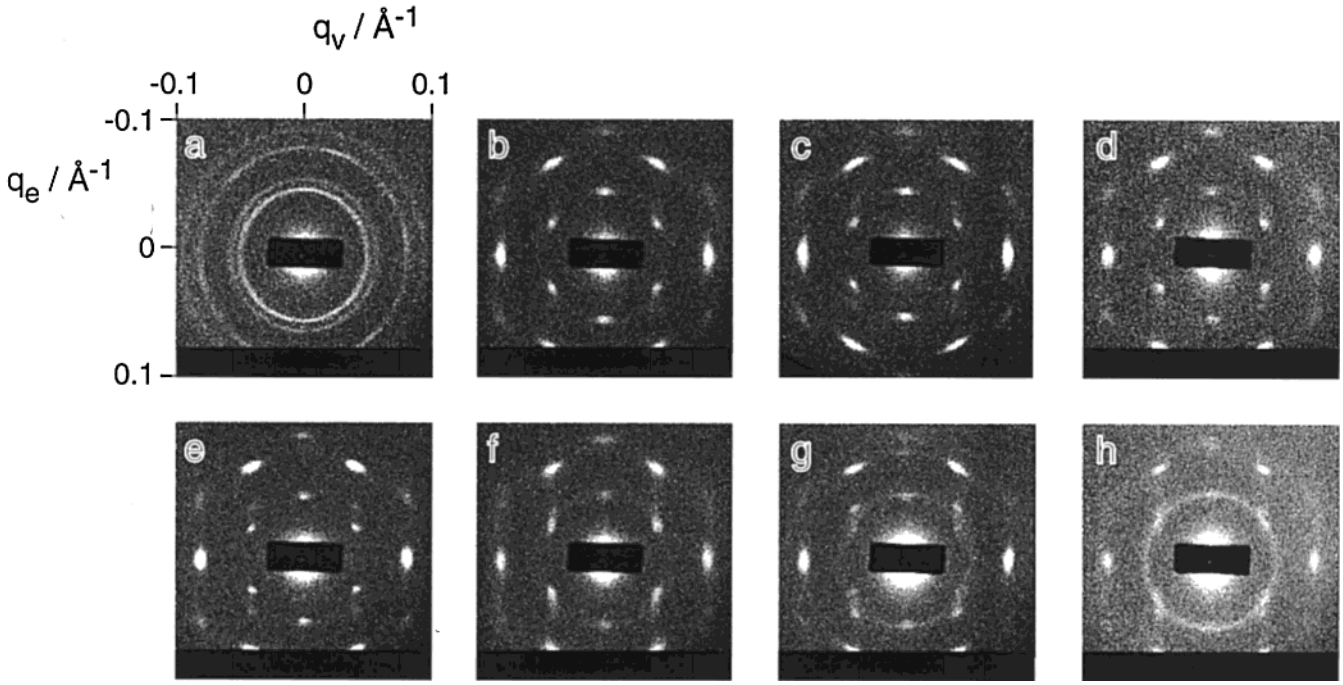

Figure 3. SAXS patterns at 20 °C in the (q_v, q_e) plane. Key: (a) sample as mounted; (b) sample during shear at $\dot{\gamma} = 5$ s^{-1}; (c) sample at rest after shear at $\dot{\gamma} = 5$ s^{-1}; (d) sample during shear at $\dot{\gamma} = 50$ s^{-1}; (e) sample at rest after shear at $\dot{\gamma} = 50$ s^{-1}; (f) sample during shear at $\dot{\gamma} = 250$ s^{-1}; (g) sample at rest after shear at $\dot{\gamma} = 250$ s^{-1}; (h) sample during shear at $\dot{\gamma} = 500$ s^{-1}. The shear direction is horizontal.

to the position of the detector (see Figure 3). The azimuthal intensity profiles were obtained by integration of the patterns in a narrow circular band centered on q^*, where q^* is the wavenumber of the first-order reflections.

For the as-mounted sample, we observe a series of diffraction rings (Figure 3a) in the positional ratio 1:$(4/3)^{1/2}$:$(8/3)^{1/2}$:$(11/3)^{1/2}$ (Figure 4a) with a first-order reflection located at $q^* = 0.0498$ Å^{-1}. This is consistent with the fcc structure ($Fm\bar{3}m$ symmetry) with a lattice parameter $a = 219$ Å and a distance between closest neighbors equal to $d = 155$ Å. The inner diffraction ring is due to {111} planes whereas the other diffraction rings are respectively due to the {200}, {220}, and {311} planes. The fcc gel is initially unoriented. By application of a steady shear rate $\dot{\gamma} = 5$ s^{-1}, orientation of the planes occurs and a 6-fold symmetry is observed for the 111 and 220 reflections (Figure 3b). The SAXS pattern obtained under shear is characteristic of an orientation of the {111} planes parallel to the shear plane. The disappearance of the 200 reflections is consistent with this orientation of the fcc structure. The presence of 6-fold symmetric reflections for both the {111} and {220} planes indicates that the structure of the gel cannot be a perfect ABCABC... stacking of hcp layers because, as mentioned in section 3.1, the 111 reflections would be absent in this case. This can be attributed to irregularities in the layer stacking and it is most likely that some ABAB... stacking sequences are also present. A close look at the azimuthal intensity profile and intensity VS q data gives us complementary information on the macroscopic orientation of domains occurring during the shearing process. In Figure 4b, we observe a decrease in q^* when the shear is applied. For the as-mounted sample, $q^* = 0.0498$ Å^{-1} while at $\dot{\gamma} = 5$ s^{-1}, $q^* = 0.0471$ Å^{-1}. This result is characteristic of a sliding of the 2D hcp layers and a similar behavior was observed for the fcc phase formed by a EPE triblock

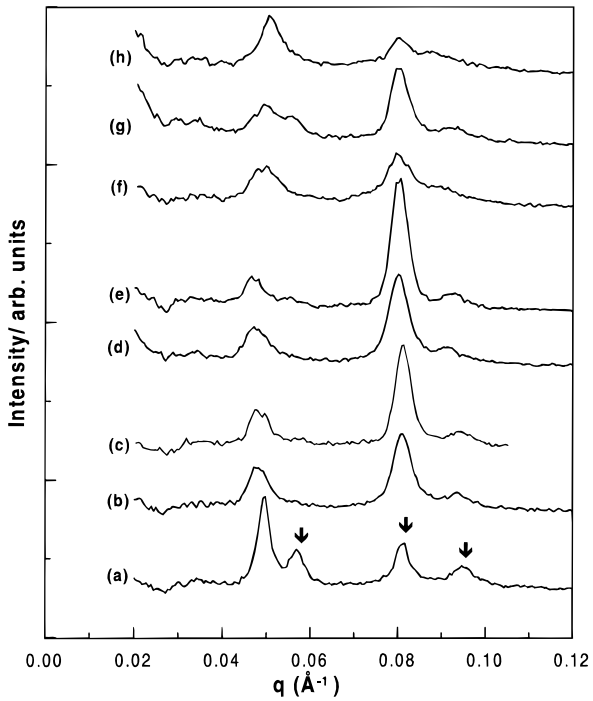

Figure 4. SAXS intensity as a function of the wavenumber, q, obtained by radial integration of the two-dimensional patterns shown in Figure 3 with $q_e \geq 0$. Key: (a) sample as mounted; (b) sample during shear at $\dot{\gamma} = 5$ s^{-1}; (c) sample at rest after shear at $\dot{\gamma} = 5$ s^{-1}; (d) sample during shear at $\dot{\gamma} = 50$ s^{-1}; (e) sample at rest after shear at $\dot{\gamma} = 50$ s^{-1}; (f) sample during shear at $\dot{\gamma} = 250$ s^{-1}; (g) sample at rest after shear at $\dot{\gamma} = 250$ s^{-1}; (h) sample during shear at $\dot{\gamma} = 500$ s^{-1}. The arrows in part a indicate the positions expected for the reflections from a fcc structure.

when subjected to steady shear[22] and has been also reported for other EB diblock gels.[9] The effect has been attributed to a decorrelation between layers that occurs

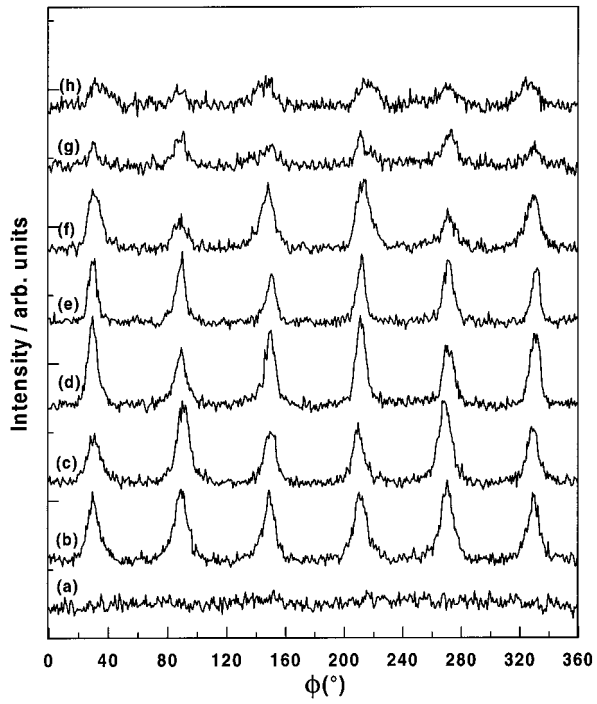

Figure 5. Profiles of the scattered intensity as a function of the azimuthal angle obtained from the SAXS patterns in Figure 3, by integration in a narrow band centered on q^*. Key: (a) sample as mounted; (b) sample during shear at $\dot{\gamma} = 5\ s^{-1}$; (c) sample at rest after shear at $\dot{\gamma} = 5\ s^{-1}$; (d) sample during shear at $\dot{\gamma} = 50\ s^{-1}$; (e) sample at rest after shear at $\dot{\gamma} = 50\ s^{-1}$; (f) sample during shear at $\dot{\gamma} = 250\ s^{-1}$; (g) sample at rest after shear at $\dot{\gamma} = 250\ s^{-1}$; (h) sample during shear at $\dot{\gamma} = 500\ s^{-1}$.

as they slide over one another.[22] In the sliding regime, the spacing between hcp layers is larger than in an fcc structure and the smallest interplanar distance in the hcp structure is $d_{hcp} = 2/\sqrt{3}d$. Using $d = 155$ Å we calculate $q^*_{hcp} = 0.0470$ Å^{-1}, which is consistent with the observed value.

Figure 5b shows that under shear at $\dot{\gamma} = 5\ s^{-1}$ the 111 reflections are equally intense while according to the LA model of sliding flow, the meridional 111 reflections are absent (see Figure 2c), independent of the variable C that is used to parametrize the relative displacement of layers, and the stacking fault parameter a, introduced in eq 2.[18] An alternative would be to invoke a zigzag model, although we do not favor this because it seems inconsistent with the observation of a reduction in q^*. Nonetheless, if we plug values into the corresponding equations in the LA model, we can obtain meridional reflections that are equally intense as the other four (eg. for $a = 0.5$). The problem is that at the same time the equatorial 220 reflections are predicted to have zero intensity, independent of a and C, as can be confirmed by analysis of the equations given by Loose and Ackerson.[18] Thus, a zigzag model is also inconsistent with the data. Instead we suggest that a significant fraction of the {111} planes are oriented perpendicular to the shear plane, i.e., in the (**v**, ∇**v**) plane, as sketched in Figure 6. These perpendicular planes must then have a random stacking sequence, to produce only meridional 111 reflections. For the 220 reflections, according to the LA model for sliding flow the equatorial reflections should be weakest, or absent in the zigzag flow model.[18] while in our case the equatorial peaks are more intense than the other four reflections. This result can be explained by the presence of a small proportion of transverse {111} planes oriented perpendicular to the shear direction, i.e., in the (**e**, ∇**v**) plane. In the absence of information in the so-called tangential configuration

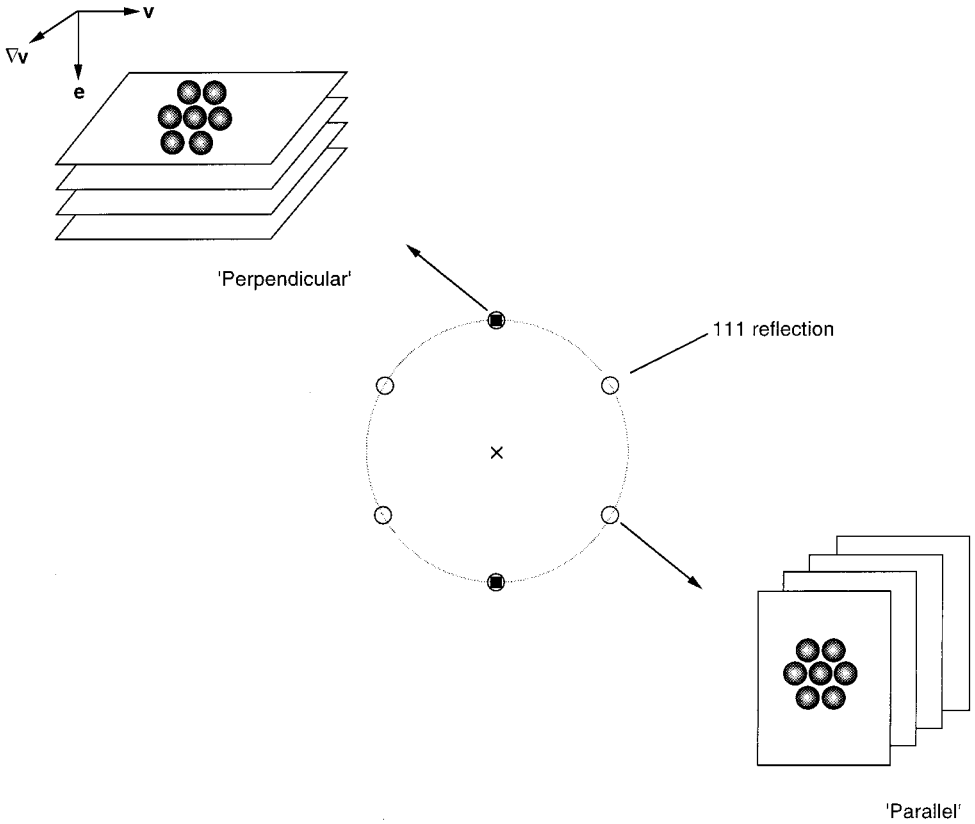

Figure 6. "Parallel" and "perpendicular" orientations of {111} planes with respect to the shear plane (**v**, **e**) that give rise to 111 reflections observed in Figure 3b.

of the Couette cell for which the X-ray beam is incident along the shear direction, our explanations of the observed SAXS patterns in terms of populations of perpendicular and transverse layers must be regarded as provisional.

We also note that meridional peaks in the outer ring of 311 reflections are stronger than the other ones. This result is consistent with a layer sliding mechanism (Figure 2c) but in contrast to the LA model, these two meridional reflections are not most intense overall. This can be explained by considering the influence of the form factor of the micelles on the layer form factor, $L(q)$ in eq 1. The form factor for an uniform spherical particle is given by

$$P(q) = V^2\left[3\left(\frac{\sin qR - qR\cos qR}{(qR)^3}\right)\right]^2 \qquad (3)$$

where V is the volume of a particle and R is its radius.

With $q^* = 0.0471$ Å^{-1} we get a value of $R = 82$ Å and with $q_{311} = 0.094$ Å^{-1}, the value of $q_{311}R$ is close to the second node of the particle form factor which is given by $qR \sim 7.72$. Thus, the intensities observed on the outer ring are lower than the intensities predicted by the sliding model which was developed without considering the particle form factor. On the other hand, the strong intensities observed for the six second-order reflections are due to a maximum of the micellar form factor.

Upon cessation of shear, the orientation of the fcc phase is mainly retained, but a few changes in the SAXS pattern shown in Figure 3c indicate that small modifications in the orientation of the structure took place. At rest, we observe four additional weak reflections close to the first order peaks and situated at ±45° from the shear direction. These reflections are 200-type reflections and can be ascribed to a reorientation of a small proportion of grains so that their {100} planes become parallel to the shear plane and their [110] direction is aligned with the shear direction. Similar orientation of grains has been previously observed for other oriented fcc gels.[20,22] The 200 reflections are too weak to appear in the intensity profile obtained by radial integration (Figure 4c). The cessation of shear is also characterized by a strong increase of the overall intensity of the 220 reflections (compare Figure 4c and Figure 4b). This result is expected since sliding stops when shearing does (compare Figure 2c and Figure 2a). It is also worth emphasising that the value of q^* does not change when shearing is stopped; i.e., the decorrelation of layers induced during the sliding of the layers is locked in. This is necessarily so because the structure has been subjected to a substantial reorganization, where the layers are further apart than in the initial powder with consequently a higher in-plane packing density. To recover the initial fcc powder would require the creation of new layers, which is (kinetically) unfavorable.

Figure 5d shows that after the shear rate is increased to $\dot{\gamma} = 50$ s^{-1}, a further decrease of the intensity of the two first-order meridional reflections occurs, together with an increase of the four other reflections. At the same time the intensity of the meridional 311 reflections increases (compare Figure 3d to Figure 3b). These variations of intensity are consistent with a propagation of the sliding mechanism to a higher number of hcp layers when the shear rate is increased. However, the variation of the 220 reflections suggests the existence of another effect. Indeed, when the shear rate is increased, the intensity of the 220 reflections increases and becomes more equally intense while the sliding model shown in Figures 1c and 2c predicts a decrease of the intensity of the 220 reflections with a lower intensity for the equatorial reflections. We can explain this behavior by considering a partial reorientation of the "perpendicular" {111} planes into an orientation parallel to the shear plane. A melting of some grains with "perpendicular" {111} planes may also occur. Both melting and reorientation of the "perpendicular" {111} planes are consistent with the decrease of the intensity of the two first-order meridional reflections. The relative reduction in intensity of the equatorial 220 reflections suggests that the initial small fraction of grains in the transverse orientation is eliminated at this shear rate.

Upon cessation of shear, four additional peaks close to the six first-order reflections are again observed (Figure 3e). As mentioned earlier, these peaks can be ascribed to a small proportion of grains having their [110] direction aligned with the shear direction. The position of the peaks is independent of the shear rate whereas their intensity increases with shear rate (compare Figure 3e and Figure 3c). The appearance of these 200 peaks at rest has been already noted previously[20,22] and was attributed to a recrystallization of grains melted during shearing. As the proportion of molten grain increases with shear rate, the proportion of grains recrystallized with their [110] direction aligned with the shear direction will also increase upon cessation of shear. We also observed by comparison of Figure 4e and Figure 4c that the overall intensity of the 220 reflections increased. After shearing at $\dot{\gamma} = 50$ s^{-1}, we obtained a maximum of hcp-type stacking along the shear gradient direction. This result is consistent with the equal intensity for each of the 111 reflections. Only a very small fraction of {111} planes remained oriented perpendicular to the shear plane.

When the shear rate is increased to $\dot{\gamma} = 250$ s^{-1}, the 1D intensity profile (Figure 4f) indicates that another flow mechanism starts to appear. At this shear rate, the maximum of the first-order peaks is observed at the same wavenumber as the first ring obtained with the unoriented sample. This behavior may be attributed to the shear melting of the hcp structure followed by a partial rearrangement into a fcc structure. Partial melting of the hcp structure is confirmed by a reduction in intensity of 220 and 311 reflections (compare Figure 4e and Figure 4f). Partial recrystallization into an fcc structure then occurs upon cessation of shear as shown by comparison of Figure 4g and Figure 4f.

When the shear rate was increased up to 500 s^{-1}, a very peculiar 2D pattern was obtained. In addition to the six reflections on the inner ring, a strong circular background is simultaneously created (Figure 3h). However, in contrast to the inner ring, six sharp 220 peaks are still present. This scattering pattern may be attributed to a partial melting of the fcc crystal. By application of a high shear rate, part of the gel has melted, producing a liquidlike scattering pattern in the inner ring but a proportion of grains still retains the fcc structure. Thus, the SAXS pattern obtained arises from a coexistence of these two phases. Upon cessation of shear, the circular ring remained (data not shown here); i.e., a nontransient melting of the fcc structure was obtained at this shear rate. We note that the sample was monitored during the SAXS experiment via a video camera linked to the beamline hutch. No evidence of

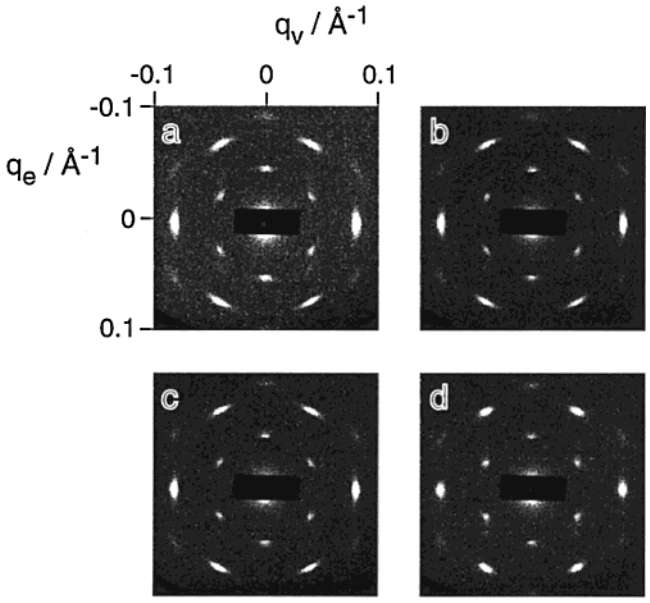

Figure 7. SAXS patterns at 20 °C in the (q_v, q_e) plane. Key: (a) sample at rest after steady shear at $\dot{\gamma} = 5$ s^{-1}; (b) sample during shear at $\dot{\gamma} = 5$ s^{-1}, $A = 1800\%$; (c) sample during shear at $\dot{\gamma} = 50$ s^{-1}, $A = 1800\%$; and (d) sample during shear at $\dot{\gamma} = 50$ s^{-1}, $A = 18\,000\%$. The shear direction is horizontal.

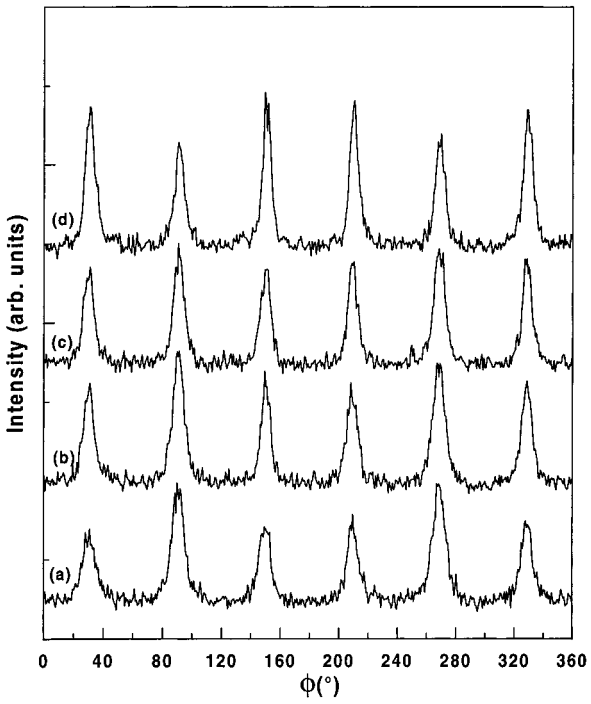

Figure 8. Profiles of the scattered intensity as a function of the azimuthal angle obtained from the SAXS patterns in Figure 7, by integration in a narrow band centered on q^*. Key: (a) sample at rest after steady shear at $\dot{\gamma} = 5$ s^{-1}; (b) sample during shear at $\dot{\gamma} = 5$ s^{-1}, $A = 1800\%$; (c) sample during shear at $\dot{\gamma} = 50$ s^{-1}, $A = 1800\%$; and (d) sample during shear at $\dot{\gamma} = 50$ s^{-1}, $A = 18\,000\%$.

Taylor instabilities or foaming was observed for the data obtained at the shear rates reported in this paper.

3.3. Oscillatory Shear Orientation. The effect of large-amplitude oscillatory shear on a gel preoriented by applying a steady shear at $\dot{\gamma} = 5$ s^{-1} was also probed by simultaneous SAXS measurements. Although the strain amplitudes applied were very large, varying the value was found to affect the flow behavior of the gel. The effect of low strain amplitudes was not explored due to the limited range of shear rates accessible with our Couette cell, although it is well-known that much lower (order unity) shear amplitudes lead to dramatic effects on sheared colloidal dispersions.[15] The two-dimensional SAXS patterns obtained in the (q_v, q_e) plane for different shear rates and shear strains are shown in Figure 7. No variation of the position of the reflections was observed for the different oscillatory shear rates and amplitudes applied to the gel. The azimuthal intensity profiles of the first-order peak are reported in Figure 8. Comparison of Figure 8b with Figure 8a shows that by application of an oscillatory shear at $\dot{\gamma} = 5$ s^{-1} and $A = 1800\%$ the intensity of the meridional 111 reflections remains constant while the intensity of the other four inner reflections increases. At the same time, the intensity of the 220 reflections increases. At a higher shear rate, up to $\dot{\gamma} = 50$ s^{-1} with the same strain amplitude, a similar distribution of intensity of the reflections was observed (Figure 8c). This effect differs from the observation made under steady shear and can be explained by a decrease of the stacking defects of "parallel" hcp layers and/or an increase of their orientation respect to the shear direction. If we consider that the meridional reflections in Figure 7a are mainly due to grains with {111} planes oriented perpendicular to the shear plane, a variation in the number of the stacking of parallel defects layers will only result in an increase of the off-meridional reflections. When the strain amplitude was increased to $A = 18\,000\%$, a different behavior is observed. The intensity of the first-order meridional reflections decreases slightly while the intensities of the other four reflections increase (compare Figure 8d and Figure 8c). At the same time a decrease of the equatorial 220 reflections is observed while the other four reflections increase. In this regime, the oscillatory shear approaches the limit of steady shear, and the intensity variation of the 111 and 220 reflections can be mainly attributed to an elimination and a reorientation of the grains with {111} planes oriented perpendicular to the shear plane, similar to the observations discussed in section 3.1.

4. Summary

The effect of steady shear or oscillatory shear on the fcc phase formed by a poly(oxyethylene)−poly(oxybutylene) diblock copolymer solution has been investigated using SAXS. Starting from an initial fcc "powder", steady shear induces the orientation of the hexagonal close-packed {111} planes both parallel and perpendicular to the shear plane. The first-order reflections shifted to a larger q^* by a fraction $2/\sqrt{3}$ compared to the unoriented fcc powder. A high degree of stacking faults was observed for the {111} planes oriented parallel to the shear plane. Under steady shear, at a low shear rate, a sliding of the hcp layers stacked along the shear gradient direction was identified For intermediate shear rates (typically 50 s^{-1}), reorientation of a fraction of the {111} planes perpendicular to the shear plane was observed while at the same time the proportion of hcp planes oriented in the shear plane increased. Upon cessation of shear, some melted grains were found to recrystallize with a [110] direction along the shear direction. Furthermore, after steady shearing at $\dot{\gamma} = 50$ s^{-1}, only a small proportion of grains with the {111} planes oriented perpendicular to the shear plane was observed. When the shear rate was increased to $\dot{\gamma} = 250$

s^{-1}, melting of the hcp structure was followed by a rearrangement into a structure resembling the initial fcc arrangement. This behavior was characterized by an increase of the wavenumber of the first-order peaks compared to the layer sliding regime. The fcc structure itself was observed to partially melt upon increasing the shear rate to $\dot{\gamma} = 500\ s^{-1}$ leading to coexistence of fcc crystallites with, presumably, a micellar liquid. In contrast to steady shear, large amplitude oscillatory shear led to a decrease of the stacking defects and/or an increase of the orientation of hcp layers with respect to the shear direction. Reorientation of the "perpendicular" {111} planes were only observed when the amplitude of oscillatory shear approached the limit of steady shear.

Acknowledgment. C.D. was supported as a postdoctoral research fellow within the EU-TMR network "Complex Architectures in Diblock Copolymer Based Polymer Systems". Beamtime at Daresbury was provided under EPSRC grant GR/L79854 to I.W.H. The Thai Government provided a Research Studentship for W.M. The EPSRC provided financial assistance for synthesis of block copolymers through grant GR/L22645.

References and Notes

(1) Hamley, I. W. *The Physics of Block Copolymers*; Oxford University Press: Oxford, U.K., 1998.
(2) Wanka, G.; Hoffmann, H.; Ulbricht, W. *Macromolecules* **1994**, *27*, 4145.
(3) Mortensen, K. *J. Phys. Condens. Matter* **1996**, *8*, A103.
(4) Alexandridis, P.; Olsson, U.; Lindman, B. *Langmuir* **1997**, *13*, 23.
(5) Alexandridis, P.; Olsson, U.; Lindman, B. *Langmuir* **1998**, *14*, 2627.
(6) Hvidt, S.; Jørgensen, E. B.; Brown, W.; Schillén, K. *J. Phys. Chem.* **1994**, *98*, 12320.
(7) McConnell, G. A.; Gast, A. P.; Huang, J. S.; Smith, S. D. *Phys. Rev. Lett.* **1993**, *71*, 2102.
(8) Gast, A. P. *Langmuir* **1996**, *12*, 4060.
(9) Hamley, I. W.; Daniel, C.; Mingvanish, W.; Mai, S.-M.; Booth, C.; Messé, L.; Ryan, A. J. *Langmuir*, in press.
(10) Mortensen, K. *Europhys. Lett.* **1992**, *19*, 599.
(11) Mortensen, K.; Brown, W.; Nordén, B. *Phys. Rev. Lett.* **1992**, *68*, 2340.
(12) McConnell, G. A.; Lin, M. Y.; Gast, A. P. *Macromolecules* **1995**, *28*, 6754.
(13) Ackerson, B. J.; Clark, N. A. *Phys. Rev. A* **1984**, *30*, 906.
(14) Ackerson, B. J.; Pusey, P. N. *Phys. Rev. Lett.* **1988**, *61*, 1033.
(15) Ackerson, B. J. *J. Rheol.* **1990**, *34*, 553.
(16) Ashdown, S.; Markovic, I.; Ottewill, R. H.; Lindner, P.; Oberthür, R. C.; Rennie, A. R. *Langmuir* **1990**, *6*, 303.
(17) Clarke, S. M.; Rennie, A. R.; Ottewill, R. H. *Langmuir* **1997**, *13*, 1964.
(18) Loose, W.; Ackerson, B. J. *J. Chem. Phys.* **1994**, *101*, 7211.
(19) Diat, O.; Porte, G.; Berret, J.-F. *Phys. Rev. B* **1996**, *54*, 14869.
(20) Pople, J. A.; Hamley, I. W.; Fairclough, J. P. A.; Ryan, A. J.; Komanschek, B. U.; Gleeson, A. J.; Yu, G.-E.; Booth, C. *Macromolecules* **1997**, *30*, 5721.
(21) Berret, J.-F.; Molino, F.; Porte, G.; Diat, O.; Lindner, P. *J. Phys. Condens. Matter* **1996**, *8*, 9513.
(22) Molino, F. R.; Berret, J.-F.; Porte, G.; Diat, O.; Lindner, P. *Eur. Phys. J. B* **1998**, *3*, 59.
(23) Hamley, I. W.; Pople, J. A.; Fairclough, J. P. A.; Ryan, A. J.; Booth, C.; Yang, Y.-W. *Macromolecules* **1998**, *31*, 3906.
(24) Hamley, I. W.; Pople, J. A.; Booth, C.; Yang, Y.-W.; King, S. M. *Langmuir* **1998**, *14*, 3182.
(25) Hamley, I. W.; Pople, J. A.; Booth, C.; Derici, L.; Imperor-Clerc, M.; Davidson, P. *Phys. Rev. E* **1998**, *58*, 7620.
(26) Hamley, I. W.; Pople, J. A.; Diat, O. *Colloid Polym. Sci.* **1998**, *276*, 446.
(27) Hamley, I. W.; Pople, J. A.; Fairclough, J. P. A.; Terrill, N. J.; Ryan, A. J.; Booth, C.; Yu, G.-E.; Diat, O.; Almdal, K.; Mortensen, K.; Vigild, M. *J. Chem. Phys.* **1998**, *108*, 6929.
(28) Pople, J. A.; Hamley, I. W.; Diakun, G. P. *Rev. Sci. Instrum.* **1998**, *69*, 3015.
(29) Bedells, A. D.; Arafeh, R. M.; Yang, Z.; Attwood, D.; Heatley, F.; Padget, J. C.; Price, C.; Booth, C. *J. Chem. Soc., Faraday Trans.* **1993**, *89*, 1235.
(30) Yu, G.-E.; Yang, Z.; Ameri, M.; Attwood, D.; Collett, J. H.; Price, C.; Booth, C.*J. Phys. Chem. B* **1997**, *101*, 4394.
(31) Heatley, F.; Yu, G.-E.; Sun, W.-B.; Pywell, E. J.; Mobbs, R. H.; Booth, C. *Eur Polym. J.* **1990**, *26*, 583.
(32) Deng, N.-J.; Luo, Y.-Z.; Tanodekaew, S.; Bingham, N.; Attwood, D.; Booth, C. *J. Polym. Sci., B: Polym. Phys.* **1995**, *33*, 1085.
(33) Derici, L.; Ledger, S.; Mai, S.-M.; Booth, C.; Hamley, I. W.; Pedersen, J. S. *Phys. Chem., Chem. Phys.* **1999**, *1*, 2773.

MA991444M